High Performance MPPT based on TS Fuzzy–integral backstepping control for PV system under rapid varying irradiance-Experimental validation

Hajar Doubabi, Issam Salhi, Mohammed Chennani, Najib Essounbouli

High Performance MPPT based on TS Fuzzy-integral backstepping control for PV system under rapid varying irradiance – Experimental validation

Hajar Doubabi [a, b,*], Issam Salhi [a], Mohammed Chennani [a], Najib Essounbouli [b]

a: Cadi Ayyad University
BP 549, Av Abdelkarim Elkhattabi, Gueliz, Marrakesh, Morocco

b : CReSTIC, Reims University
9 rue de Québec B.P 396, F-10026, Troyes cedex, France

hajardoubabi@gmail.com, isalhi@yahoo.fr, medchennani@gmail.com, najib.essounbouli@univ-reims.fr

* Corresponding authors.
Tel.: +212 666 256 57

High Performance MPPT based on TS Fuzzy-integral backstepping control for PV system under rapid varying irradiance – Experimental validation

Abstract

With the recent focus marked on energy efficiency and solar energy development, much research is being dedicated to the development of enhanced maximum power point tracking (MPPT) algorithms for photovoltaic applications. However, the main criteria with regard to tracking performances and circuit implementation are still considered as a major challenge under rapid varying weather conditions. In this paper, a T-S Fuzzy- integral backstepping-based hybrid MPPT technique is proposed for rapid, accurate and efficient tracking. The proposed technique enables reliable and stable operation under fast dynamic environmental changes. Besides, it is simple as it does not require extra atmospheric sensors. The theoretical analysis addressed in this study is verified through simulations via Matlab/Simulink and experimental outdoor tests. A comparison with different other MPPT techniques is provided to highlight the performances of the developed MPPT method.

Keywords: Maximum power point tracking; Integral Backstepping; Takagi-Sugeno Fuzzy; Photovoltaic system; DC-DC boost converter.

I. Introduction

The global environmental harm, due to fossil fuels use, has led to an increased need for alternative power sources. In recent years, the transition to renewable energy sources has received greater consideration in various sectors owing to their incredible reduction of greenhouse gas emissions. Solar energy is a free, clean and inexhaustible source of power, which makes it a reliable means of supplying electricity to the world. Solar photovoltaic (PV) systems provide electric power by directly converting solar irradiance into electricity. PV systems are used in various applications and can produce power at levels of few watts to megawatts. The electrical characteristic of the PV system is non-linear and varies with the atmospheric conditions. Hence, ensuring the efficient generation of maximum power, especially for situations with rapidly changing irradiation conditions, is considered the main challenge.

Maximum power point tracking is a fundamental control strategy used to harvest the highest photovoltaic power under all environmental conditions. In general, MPPT algorithms are incorporated into switching power converters to provide the maximum available power from panels. Specifically, the converter is utilized as an adapting stage between the PV module and the load, so by controlling its duty ratio, the PV system could operate at the maximum power point (MPP) in spite of climate changes.

Several MPPT techniques have been developed in the literature [1]. Perturb and observe (P&O) and incremental conductance (IC) are reviewed as conventional MPPT methods [2-3]. The P&O method is widely investigated due to its simplicity of implementation, but it introduces considerable oscillations near to the MPP that lead to power losses. On the other hand, the IC method is more flexible and accurate than the P&O. Nevertheless, it has as a main drawback the control circuit complexity that results in high response time to reach the MPP. However, the above-mentioned MPPT algorithms generally fail in tracking effectively the MPP under varying solar irradiation. These have led the researchers to explore and discover new soft computing techniques for enhanced MPPT controller performances.

Genetic Algorithm (GA) [4], Particle Swarm Optimization (PSO) [5], Random Search methods [6], Ant Colony Optimization [7] and Shuffled Frog Leaping Algorithm [8] are bio-inspired and population-based global search algorithms that have been proposed for MPPT control. They can well cope with different atmospheric conditions and track the MPP efficiently. However, these techniques present weak dynamic performances and long processes that increase the computational complexity. In addition, they exhibit a trade-off between convergence accuracy and convergence speed, making the choice of the population size, chromosome and the number of iterations very critical and need adjustment according to irradiation conditions.

Artificial intelligence algorithms such as artificial neural network (ANN) [9] and Fuzzy logic control (FLC) [10] have been also used for the MPPT control. They can successfully mitigate the shortcomings of the conventional algorithm namely the oscillations around MPP and the tracking speed. Moreover, the robust design of these techniques plays a key role in solving the nonlinearity and uncertainties problems of the PV system. However, the ANN method requires large data and suffers from high training time that results in a complex network and decreases the accuracy in MPPT. A comparative study has been conducted experimentally in [11] revealing that the MPPT controller based on FLC extracts more PV power than the one using ANN. Even though, the FLC may fail to converge under rapid dynamic irradiance

changes. Therefore, it is recommended to be combined with other techniques to achieve more attractive performances and reliable MPPT control [12].

Most power converters that incorporate the MPPT algorithm in the PV system applications are nonlinear in nature, which has led researchers to think of advanced nonlinear controllers guaranteeing high convergence speed and robustness for MPPT under varying atmospheric conditions. Several researchers have tried to perform a high efficient MPPT algorithm using sliding mode (SM) control [13-14]. This latter ensures the stability and robustness of the system; however, the chattering phenomena, the variable switching frequency and the significant steady-state error are the major shortcomings of the method. Therefore, other studies have included an integral action term in order to mitigate these associated SM control problems [15-16]; however, undesirable disturbances and high overshoots are observed. These limitations have led researchers in [17] to propose a novel adaptive integral derivative SM - based strategy to enhance the dynamic response of MPPT and increase the PV power harvest under fast irradiation changes. However, the simulation and experimental validation of this method have been conducted only over a limited range of irradiance [500W/m²-1000W/m²]; while the performance evaluation is more substantive under high irradiance variations. Moreover, the SM control generally requires a priori knowledge about the uncertainty bounds, considered also as a main drawback. Reference [18] proposes a Lyapunov based single-loop controller for MPPT of a standalone PV system. The asymptotic stability of the overall system is demonstrated. Nevertheless, the effects of climate variations have not been taken into consideration in the practical validation of the developed MPPT technique. An intelligent non-linear discrete-PID controller is synthetized in [19] for MPPT of the photovoltaic module. This method maintains the properties of the classic PID controller where the derivative and integral terms are discretized based on the Forward Euler Formula. PSO and GA are used to select adequate gains of the controller. However, this technique is not validated experimentally. In [20], an MPPT technique based on model predictive control was developed to extract the maximum available PV power at divers weather conditions. Nevertheless, this method faces considerable oscillations under abrupt irradiance changes. The nonlinear integral backstepping method is well known for both its excellent dynamic response and it ensures global asymptotic stability. Therefore, it has been proposed for MPPT in [21], for a system consists of a PV array, buck-boost converter and load resistor. It is revealed that this method could be a suitable candidate for MPPT control under challenging environmental conditions as high dynamic performances are achieved. However, the experimental validation of this technique is not addressed. Furthermore, the MPP location is

estimated using basic linear approximations, that are not able to precisely determine the MPP locus under changing weather conditions, which results in significant power loss [1] [22].

In light of the above discussion, the present work proposes a high-performance MPPT method using Takagi-Sugeno (TS) fuzzy combined with nonlinear integral backstepping control. Specifically, the contributions of this paper are as follow:

1) Designing a novel MPP approximator based on TS fuzzy technique for estimating, with higher precision, the exact MPP locus.
2) Developing an integral backstepping controller that enforces the PV system to generate the desired power by acting on the boost converter duty cycle.
3) The proposed MPPT method is supported by detailed mathematical investigation and validated through both simulations in MATLAB/Simulink and experimental tests using the dSPACE (DS1104) interface.
4) The performance of the proposed MPPT algorithm is examined under low/high irradiation levels, gradual/abrupt/step-up/step-down irradiation variations and dynamic test standard EN50530.
5) Comparison of the developed MPPT method to the existing ones (P&O, modified incremental conductance (MIC), PSO and a hybrid controller combines P&O with fractional-order proportional-integral (P&O-FOPI)) under varying irradiance profile.

The findings show that the proposed technique successfully monitors different dynamic variations of irradiation and achieves high accuracy in locating MPP, fast convergence velocity, zero steady-state error, stable operation and high MPPT efficiency. Moreover, the structure of the proposed MPPT controller is simple to implement and doesn't require environmental sensors, which makes it applicable for most PV system configurations.

This research paper is structured as follows: Section II presents the overall structure of the proposed solar battery charging system and describes the MPPT technique in detail. Simulations and experimental results are discussed in Section III. Concluding remarks are drawn in the last section.

II. Overview of the proposed PV system

Figure 1 illustrates the structure of the proposed MPPT-based solar battery charging system. It comprises mainly a PV array and a battery load that are interconnected via a boost type DC-DC converter controlled by the proposed MPPT algorithm.

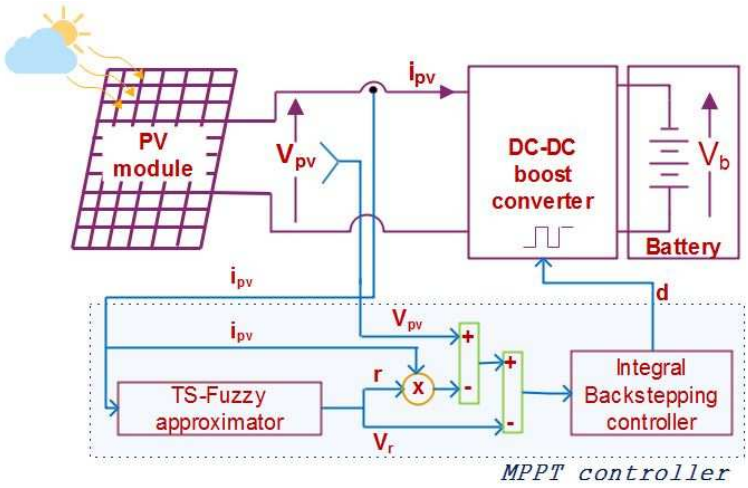

Fig.1. Block diagram of the PV battery charging system with the proposed MPPT control loop

II. 1. PV modeling

A PV module is generally made by the connection of PV cells in parallel and series to achieve the required output current and voltage. In the literature, different equivalent models have been introduced to represent the PV cell operation. The most popular one is the "single-diode model" depicted in Fig.2. It typically composed of a current source, a diode and series/parallel resistances [23]. The electrical circuit can be mathematically described by the following equations

$$I_o = I_{ph} - I_d = I_{ph} - I_{rsc}\left[\exp\left(\frac{V_o}{V_{th}}\right) - 1\right] \tag{1}$$

where I_{rsc} is the reverse saturation current and V_{th} is the thermal voltage of the diode. The generated photocurrent I_{ph} is expressed linearly with the solar irradiation (G) as follows

$$I_{ph} = \left[I_{sc\_STC} + K_{sc}\left(T_{cell} - T_{cell\_STC}\right)\right]\frac{G}{G_{STC}} \tag{2}$$

where I_{sc_STC} is the cell short circuit current measured at Standard Test Condition (STC), T_{cell_STC} is 25°C, G_{STC} is 1000W/m², and K_{sc} is the short circuit current coefficient. The diode current is given by

$$I_d = \left[I_{rsc\_STC}\left(\frac{T_{cell}}{T_{cell\_STC}}\right)^3 \exp\left\{\frac{q \times E_G}{k_B \times A}\left(T^{-1}_{cell\_STC} - T^{-1}_{cell}\right)\right\}\exp\left\{\frac{q \times V_o}{k_B \times A \times T_{cell}} - 1\right\}\right] \tag{3}$$

where I_{rsc_STC} is the reverse saturation current at STC, k_B: Boltzmann's constant, q: the charge of electron, E_G: the band-gap, and A: the diode ideality factor.

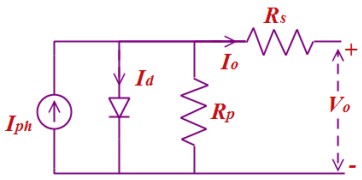

Fig. 2. PV cell equivalent model

The electrical parameters of the PV module adopted in this work, provided at STC (i.e.1000W/m², 25°C) are tabulated in Table I.

Table I: Electrical characteristics of the used PV module

Parameters	***Value***
Maximum power P_{mpp}	62W
Output power tolerance	±5%
Voltage at maximum power point V_{mpp}	13.23 V
Open circuit voltage V_{oc}	19.0 V
Short circuit current I_{sc}	5.8 A
Current at maximum power point I_{mpp}	4.68 A
No. of cells and connections	36 (4x9)

II. 2. Boost-type DC-DC converter

The boost converter (or step-up converter) is utilized to convert the lower dc input voltage provided by the PV module (V_{pv}) to higher dc output voltage for the battery charging (V_b), which is the load. As shown in Fig. 3, the circuit topology of the converter consists mainly of an inductor L, input and output capacitors (C_i & C_o), a power switch MOSFET M and a diode D. Table II gives the parameters values of the designed boost converter. The equations characterizing these parameters are expressed as follows

$$\left.\begin{aligned} V_b &= V_{pv}\left(\frac{1}{1-d}\right) \\ L &= \frac{V_{pv}\times\left(V_b - V_{pv}\right)}{\Delta I_{ripple}\times f_s \times V_b} \\ C_o &= \frac{I_b \times d}{f_s \times \Delta V_{ripple}} \end{aligned}\right\} \quad (4)$$

where d is the duty cycle, ΔI_{ripple} is the inductor ripple current, ΔV_{ripple} is the output voltage ripple and f_s is the switching frequency.

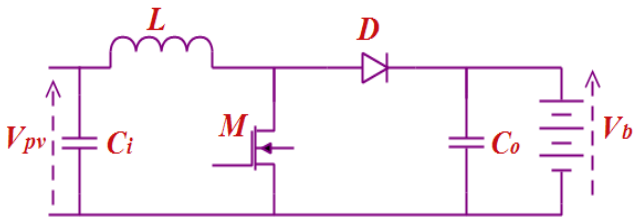

Fig. 3. Boost type DC-DC converter structure

The converter is considered operating under continuous conduction mode. The mathematical equations modeling the converter in the ON and OFF states of the switches are formulated in (5) and (6), respectively

$$\left.\begin{aligned} \frac{dV_{pv}}{dt} &= \frac{I_{pv}}{C_i} - \frac{I_L}{C_i} \\ \frac{dI_L}{dt} &= \frac{V_{pv}}{L} \end{aligned}\right\} \text{(M- ON, D- OFF)} \tag{5}$$

$$\left.\begin{aligned} \frac{dV_{pv}}{dt} &= \frac{I_{pv}}{C_i} - \frac{I_L}{C_i} \\ \frac{dI_L}{dt} &= \frac{V_{pv}}{L} - \frac{V_b}{L} \end{aligned}\right\} \text{(M-OFF,D-ON)} \tag{6}$$

where I_{pv} is the generated PV current and I_L is the inductor current.

Table II: Boost converter specifications

Parameters	***Value***
Inductor (L)	300µH
Capacitors (C_i , C_o)	440 µF, 100 µF
Switching frequency (f_s)	30 kHz
Ripple current (ΔI_{ripple})	1.6 A
Ripple current (ΔV_{ripple})	0.1 V

II. 3. Proposed MPPT controller

The proposed MPPT technique includes two stages as shown in Fig.1. The premier one based on the TS fuzzy approach takes place to continuously determine the MPP position corresponding to the irradiance level, and hence generates the setpoint (V_{pv}^{ref}). The second one based on the nonlinear integral backstepping method enforces the operation point to efficiently track the desired MPP (setpoint) using the synthesized control law.

II. 3.1. TS Fuzzy approximator

The PV current (I_{pv}) hugely varies with the solar irradiance variation, which affects the MPP location as shown in Fig.4. If the MPPs corresponding to different irradiance levels are connected together, then, an MPP trajectory is obtained. This trajectory is generally nonlinear; therefore, segmentation could be used to decompose it into a number of segments. Then, each line segment is extended to get the so-called MPP lines as illustrated in Fig.4. It is interesting to note that the MPP lines have different slopes and voltage axis- intercepts. Hence, each MPP line can be expressed mathematically as

$$V_{pv} - r_i . I_{pv} - V_{r_i} = 0 \tag{7}$$

where r_i is the corresponding slope line, V_{r_i} is the voltage axis- intercept and *i=1, 2…n; n* is the MPP line number. Based on the MPP lines data, the proposed MPPT controller can accurately estimate the MPP locus at any given solar irradiance using the T-S fuzzy approach as introduced in the following:

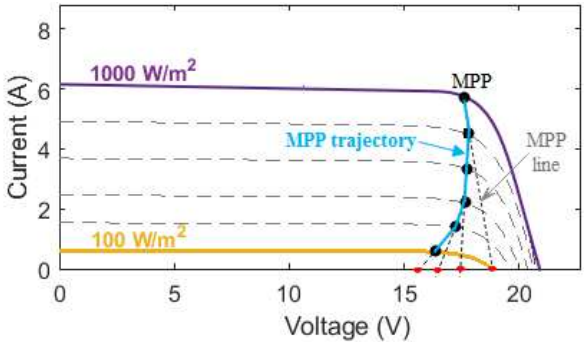

Fig. 4. The MPP trail under different irradiance levels based on I-V characteristic of the PV array

As the PV current parameter (I_{pv}) enables the detection of the irradiance intensity, it has been identified as an input of the fuzzy inference system that process it employing pre-specified fuzzy rules to produce the corresponding outputs r and V_r.

For typical values of I_{pv} , the fuzzy inference rules have the form in Eq.8,

$$R^i: \quad \text{IF } I_{pv_i} \text{ is } \sigma_i \quad \text{THEN } r_i \text{ and } V_{r_i} \tag{8}$$

where *i=1, 2…n; n* is the number of inference rules (corresponding to MPP lines), σ_i is the fuzzy set. The premise variable I_{pv} is a measurable variable of the system. Crisp input data is converted into fuzzy values using membership functions. In this study, the number and value of each membership function were selected depending on the collected data from the PV system. The shape of membership functions has been decided using the trial-and-error method.

Using a standard fuzzy inference method that uses singleton fuzzifier, product inferred, and weighted average defuzzifier, the fuzzy system inferred outputs are

$$\begin{cases} r = \dfrac{\sum_{i=1}^{n} \mu_i(I_{pv_i}) r_i}{\sum_{i=1}^{n} \mu_i(I_{pv_i})} \\ V_r = \dfrac{\sum_{i=1}^{n} \mu_i(I_{pv_i}) V_{r_i}}{\sum_{i=1}^{n} \mu_i(I_{pv_i})} \end{cases} \tag{9}$$

where μ is the normalized membership function and $\mu_i(I_{pv_i}) \Big/ \sum_{i=1}^{n} \mu_i(I_{pv_i}) \geq 0$ are the normalized weights.

II. 3.2. Integral backstepping controller

The nonlinear integral backstepping control method aims to let the PV panel output voltage (V_{pv}) reach the maximum voltage (V_{pv}^{ref}) by adjusting the boost converter duty cycle. V_{pv}^{ref} is considered as a reference voltage and expressed by $V_{pv}^{ref} = V_r + r.I_{pv}$

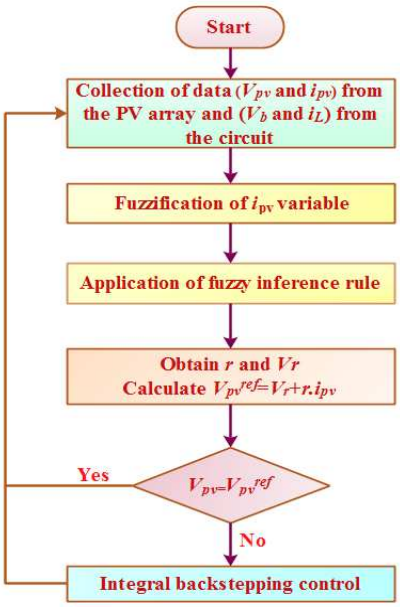

Fig. 5. Flowchart structure of the proposed MPPT control

Using (5) and (6), the V_{pv} voltage and the inductor current I_L are defined as state variables of the system x_1 and $x_2$respectively, the corresponding 2-D differential equation is set as shown in (10).

$$\begin{cases} \dot{x}_1 = \dfrac{I_{pv}}{C_i} - \dfrac{x_2}{C_i} \\ \dot{x}_2 = \dfrac{x_1}{L} - (1-d)\dfrac{V_b}{L} \end{cases} \tag{10}$$

where d ϵ [0, 1] and is the control signal.

The general objective of the integral backstepping method is to stabilize the system states at the origin considered as the equilibrium point. Its algorithm is based on reclusively defining some states as "virtual controls" to get the ultimate control laws using the control Lyapunov function. The main merit of this method is the asymptotic stability and nonlinearities elimination. For this system, two steps are required to obtain the control law "d".

*Step1:*The error z_1 between the state variable x_1 and the reference V_{pv}^{ref} is set as follow

$$z_1 = x_1 - V_{pv}^{ref} \tag{11}$$

The second errorz_2 between $x_2$that is considered as a virtual control input of the system in (10) (or a reference of the inner loop) and the stabilizing function α_1 is given by

$$z_2 = x_2 - \alpha_1 \tag{12}$$

Calculating the derivative of z_1 in (11) with respect to time, and by using (12) and the model in (10), we obtain

$$\dot{z}_1 = -\frac{1}{C_i} z_2 - \frac{1}{C_i} \alpha_1 + \frac{1}{C_i} I_{pv} - \dot{V}_{pv}^{ref} \tag{13}$$

Integral action is introduced into the error term as

$$e_1 = z_1 + \psi \tag{14}$$

where
$$\psi = \int_0^t \left(x_1 - V_{pv}^{ref} \right) dt = \int_0^t z_1 dt \tag{15}$$

According to the definition of the Lyapunov function provided in [24], the first Lyapunov function is chosen to be globally positive definite as follow

$$V_1 = \frac{1}{2} z_1^2 + \frac{a}{2} \psi^2 \tag{16}$$

where a is a positive definite real number.

The time derivative of V_1 is

$$\begin{aligned} \dot{V}_1 &= z_1 \dot{z}_1 + a\psi\dot{\psi} \\ &= z_1 \left(-\frac{1}{C_i} z_2 - \frac{1}{C_i} \alpha_1 + \frac{1}{C_i} I_{pv} - \dot{V}_{pv}^{ref} + a\psi \right) \end{aligned} \tag{17}$$

$\dot{V}_1$ must be negative definite to guarantee a global asymptotic stability. This can be imposed by taking the stabilizing function as

$$\alpha_1 = C_i k_1 z_1 + I_{pv} - C_i \dot{V}_{pv}^{ref} + C_i a\psi \tag{18}$$

From (13) and (18), we obtain

$$\dot{V}_1 = -k_1 z_1^2 - \frac{1}{C_i} z_1 z_2 \tag{19}$$

$$\dot{z}_1 = -k_1 z_1 - \frac{1}{C_i} z_2 - a\psi \tag{20}$$

Where $k_1$is a constant and positive parameter, then the stability is verified. It is worth mentioning that the term $\frac{1}{C_i} z_1 z_2$ will be eliminated automatically in the next step.

Step2: From (12), the time derivative of the second error z_2 can be expressed as

$$\dot{z}_2 = \dot{x}_2 - \dot{\alpha}_1 \tag{21}$$

Substituting (10) into (21) yields to

$$\dot{z}_2 = \frac{1}{L} x_1 - \frac{1}{L} V_b + \frac{d}{L} V_b - \dot{\alpha}_1 \tag{22}$$

The time derivative of the stabilizing function α_1 is obtained as

$$\begin{aligned} \dot{\alpha}_1 &= C_i k_1 \dot{z}_1 + \dot{I}_{pv} - C_i \ddot{V}_{pv}^{ref} + C_i a \dot{\psi} \\ \dot{\alpha}_1 &= C_i (a - k_1^2)(x_1 - V_{pv}^{ref}) - k_1 (x_2 - \alpha_1) + \dot{I}_{pv} - C_i \ddot{V}_{pv}^{ref} - C_i k_1 a \psi \end{aligned} \tag{23}$$

The second Lyapunov function is chosen with similar proprieties as (16)

$$V_2 = V_1 + \frac{1}{2} z_2^2 \tag{24}$$

The Lyapunov function (24) derivative with respect to time is

$$\dot{V}_2 = \dot{V}_1 + z_2 \dot{z}_2 \tag{25}$$

Substituting (19) and (22) into (25) yields to

$$\dot{V}_2 = -k_1 z_1^2 + z_2 \left(-\frac{1}{C_i} z_1 + \frac{1}{L} x_1 - \frac{1}{L} V_b + \frac{d}{L} V_b - \dot{\alpha}_1 \right) \tag{26}$$

To ensure stability, the $\dot{V}_2$value must be negative definite and keep $\dot{V}_2 = -k_1 z_1^2 - k_2 z_2^2$. This can be achieved if

$$-k_2 z_2 = -\frac{1}{C_i} z_1 + \frac{1}{L} x_1 - \frac{1}{L} V_b + \frac{d}{L} V_b - \dot{\alpha}_1 \tag{27}$$

Where $k_2$is a constant and positive parameter, from (22) and (27), we obtain

$$-k_2 z_2 = -\frac{1}{C_i} z_1 + \dot{z}_2 \tag{28}$$

Thus, $\dot{z}_2$ is given by

$$\dot{z}_2 = -k_2 z_2 + \frac{1}{C_i} z_1 \tag{29}$$

By solving equation (27) and using (23), the control input of the system is

$$\begin{aligned} d = x_1 \left[\frac{L}{C_i V_b} - \frac{1}{V_b} + \frac{LC_i}{V_b}(a - k_1^2) + \frac{L}{V_b} C_i k_1 (k_1 + k_2) \right] + x_2 \left[-\frac{L}{V_b}(k_1 + k_2) \right] + \\ V_{pv}^{ref} \left[-\frac{L}{V_b C_i} - \frac{LC_i}{V_b}(a - k_1^2) - \frac{L}{V_b} C_i k_1 (k_1 + k_2) \right] + I_{pv} \left[\frac{L}{V_b}(k_1 + k_2) \right] - \\ \dot{V}_{pv}^{ref} \left[\frac{L}{V_b} C_i (k_1 + k_2) \right] + \dot{I}_{pv} \frac{L}{V_b} - \ddot{V}_{pv}^{ref} \frac{L}{V_b} C_i + \psi \left[-\frac{L}{V_b} C_i k_1 a + \frac{L}{V_b} C_i (k_1 + k_2) a \right] + 1 \end{aligned} \tag{30}$$

where $0 \prec d \prec 1$.

The flowchart structure of the proposed MPPT control is described in Fig.5.

Using (20) and (29), the new system model expressed in the coordinates (z_1, z_2) can be given by (31)

$$\dot{z} = \underbrace{\begin{bmatrix} -k_1 & -\frac{1}{C_i} \\ \frac{1}{C_i} & -k_2 \end{bmatrix}}_{[A]} z + \begin{bmatrix} -a\psi \\ 0 \end{bmatrix} \tag{31}$$

The matrix $[A]$can be decomposed as follow

$$\begin{aligned} [A] &= -\begin{bmatrix} k_1 & 0 \\ 0 & k_2 \end{bmatrix} + \begin{bmatrix} 0 & -\frac{1}{C_i} \\ \frac{1}{C_i} & 0 \end{bmatrix} \\ [A] &= -[M_d] + [M_a] \end{aligned} \tag{32}$$

where $[M_d]$ is a diagonal matrix and $[M_a]$ is an anti-symmetric matrix.

$[M_a] = \frac{1}{2}\left([A] - [A]^T\right), [M_a]^T = -[M_a], [M_d] = \frac{1}{2}\left([A] + [A]^T\right)$ and $z^T [M_a] z = 0 \; \forall z \neq 0$. Since $V_2 = \frac{1}{2} z^T z$ thus $\dot{V}_2 = z^T \dot{z} = z^T (-[M_d] z + [M_a] z) = -z^T [M_d] z \prec 0$

This implies that (z_1, z_2) = (0, 0) results to be an equilibrium point of the closed-loop system. This ultimately results in $x_1 = V_{pv}^{ref}$ and $x_2 = I_{pv}$. The obtained condition $\dot{V}_2 = -z^T [M_d] z \prec 0$ proves the global asymptotical stability of the system. Specifically, by using the control signal deduced in (26), the proposed backstepping controller stabilizes the PV panel voltage V_{pv} to the desired reference voltage V_{pv}^{ref} as $t \to \infty$.

III. Results and discussions

An experimental test has been firstly carried out to plot the I-V characteristic of the PV panel under different sun irradiance. The measurements were carried out in clear weather) on November 10, 2019, in Marrakesh city, Morocco. The irradiance was recorded using a pyranometer oriented and tilted at the same angle as the PV module. The equipment typically used in such experiment is current and voltage sensors as well as an adjustable resistor with high value to meet the open-circuit condition. The current and voltage provided by the PV panel change by varying the resistor, which shifts the operating point on the PV panel characteristics. Figure 6 illustrates the resulted experimental data. The measurement uncertainties generally come from instrumentation and calibration. In this test, the uncertainty of the employed voltage and current sensors is estimated to be ±0.1%.

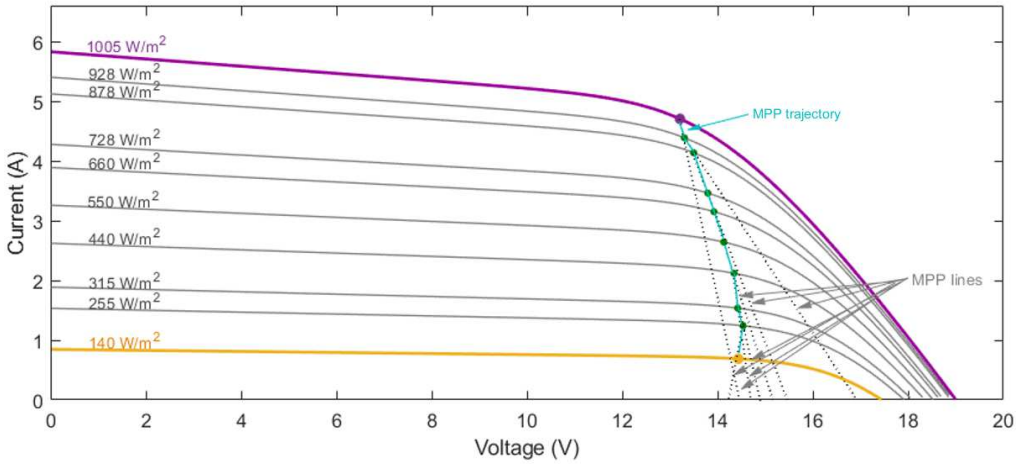

Fig.6. Experimental I-V characteristic of the PV panel for different irradiance levels

Based on the MPP lines and the resulted MPP trail marked in Fig.6, the fuzzy system parameters are set; namely the number of inference rules *n=7*, the membership functions for the i_{pv} variable portrayed in Fig.7.

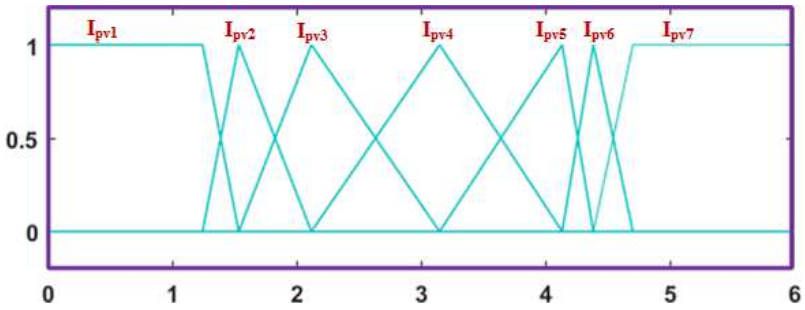

Fig.7. Membership functions for the PV current

In this work, the TS Fuzzy approximator was built using the fuzzy logic controller block (FLCB) of Matlab/Simulink, as depicted in Fig.8. The FLCB enables easy implementation and flexible configuration of the fuzzy interference system. The input of the FLCB is the PV current I_{pv} . The outputs are the corresponding slope r and voltage axis- intercept V_r of MPP line. To perform the experimental tests, the presented simulink block diagram of the proposed controller can be implemented in the dSPACE's real-time interface (RTI) where a C code is automatically generated, downloaded and executed by the Real-Time Workshop in conjunction with the dSPACE's Real-Time Interface.

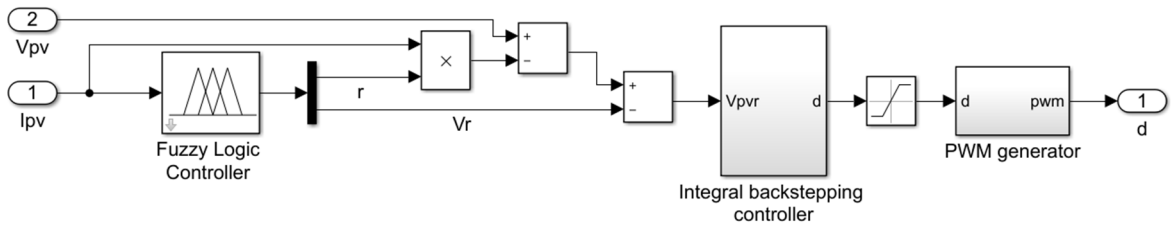

Fig. 8. Simulink block diagram of the proposed MPPT controller

III. 1. Simulation validation

In order to confirm the effectiveness of the proposed MPPT controller, simulation tests have been performed in Matlab/Simulink on the solar charging battery system depicted in Fig.1. Different dynamic variations of irradiance were examined, the MPPT controller performance was evaluated through the EN50530 dynamic test standard and a comparison to other existing MPPT controllers was provided.

III. 1.1.Simulation results under solar irradiance fluctuations

The proposed MPPT controller performances were firstly verified through an irradiance profile comprising different changes as depicted in Fig.9.a. The simulation results are plotted in Fig.9. In the beginning, the PV module received a constant irradiance of 100W/m^2 for 126ms. A fast start-up transient of only 0.4ms without overshoots is achieved

and the corresponding maximum PV power is produced as illustrated in Fig.9.d. Then, an abrupt step-up irradiance change (from 100W/m² to1000W/m^2) has been taken place. As a result, the controller successfully tracks the new MPP and the generated power instantly changed from 7.1W to 61.5W. The enlarged waveform in Fig.9.d shows the fast transient response and the stability achieved with the proposed MPPT method. The irradiance value remained at 1000W/m² for 224ms. Afterward, the irradiance followed a decreasing ramp of gradient 1800W/m^2/s to reach 100W/m^2 at 850ms and an increasing ramp with the same gradient starts at 1.3s to reach 1000W/m^2 at 1.8s. This profile can be frequently faced in real-life, for example, under moving clouds. During these gradual changes of irradiance, the MPP is steadily and accurately tracked; hence, the PV system keeps producing the maximum available power according to the irradiance intensity as shown in Fig.9.d. Moreover, the oscillation around MPP that results in energy losses is avoided. It can be also noticed from Fig.9.b that the voltage V_{pv} is forced to stick at the MPP by following the reference voltage V_{pv}^{ref} curve quite perfectly. Thus, the operating point is restricted from being diverted. This is achieved thanks to the proposed MPPT mechanism described earlier. The TS fuzzy approximator continuously located the exact peak power voltage (V_{pv}^{ref}) according to the irradiance intensity, which is efficiently tracked using the integral backstepping controller.

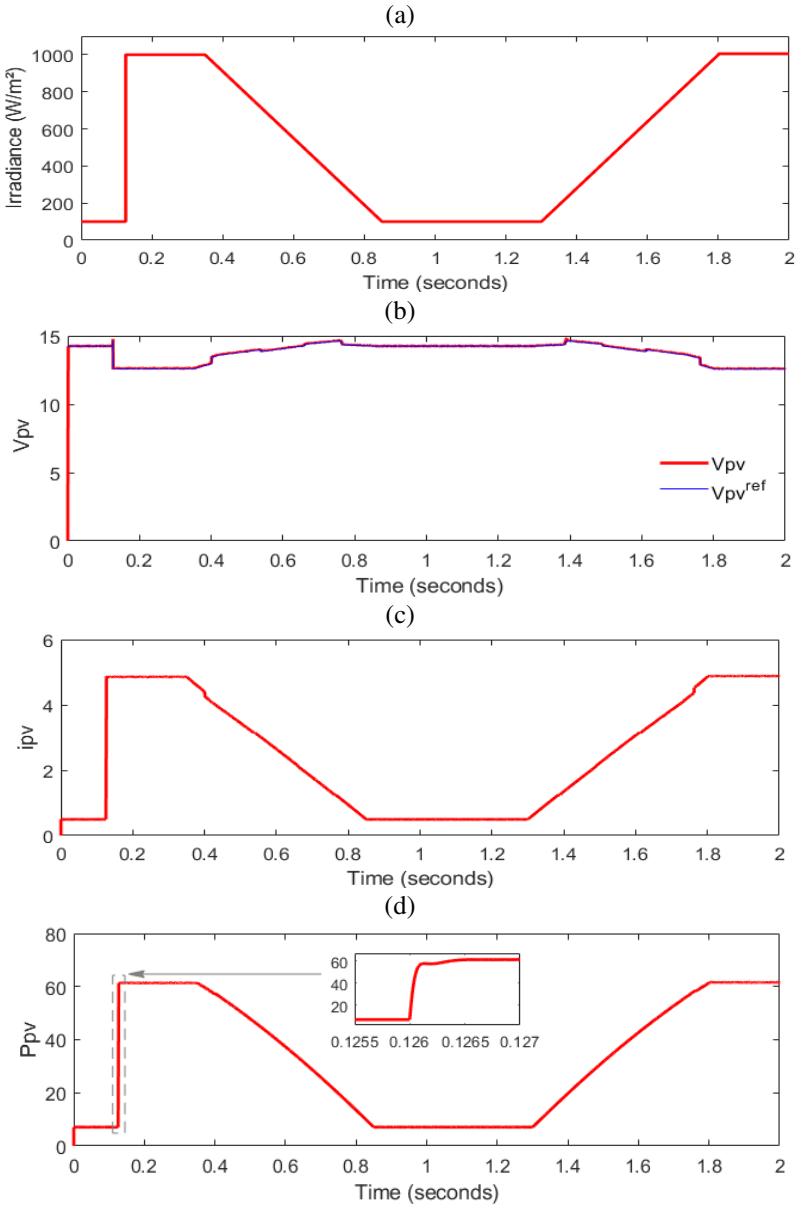

Fig. 9. Performance of the proposed MPPT controller under changing irradiance (a) Solar irradiance profile (b)PV array voltage compared to the setpoint V_{pv}^{ref} (c) PV array current (d) generated power by the PV array

In general, the PV system continuously experiences changes in irradiance. Hence, when the PV system is installed under real outdoor conditions, the long-term production investment benefits would be affected by the dynamic MPPT performance. In this regard, the EN50530 dynamic test standard defines a procedure to investigate and quantify the proposed MPP tracker dynamic performance [25]. The procedure is based on testing the controller under several irradiation ramp sequences with different irradiance levels and slopes ($\Delta G/\Delta t\left[W/m^2 s\right]$). Specifically, irradiation changing ramps from 10% to 50%, 30% to 100%, and 1% to 10% of STC irradiation level have to be applied with slopes ranging from 0.5 W/m²/s to 50W/m²/s, 10W/m²/s to 100W/m²/s and 0.1W/m²/s respectively. As part of the test sequence results,

Fig.10 depicts the PV power obtained in case of dynamic irradiation changes from 300W/m² to 1000W/m² using a slope of 100W/m²/s. This test highlights the excellent performance of the proposed MPPT method. As inferred from the resultant waveforms, the proposed controller follows perfectly the correct tracking sense and ensures the global PV system stability even under successive dynamic irradiation changes. The energy losses are low due to the reliability and fast convergence speed of the proposed technique. Accordingly, this has been evaluated by the calculation of the dynamic MPPT tracking efficiency mathematically defined by Eq.33, where $P_{pv}(t)$ is the extracted power from the PV array, $P_{MPP}(t)$ is the theoretical PV power at the MPP and T_{MPP} is the total period of calculation.

$$\eta_{dyn,MPPT} = \frac{\int_0^{T_{MPP}} P_{pv}(t).dt}{\int_0^{T_{MPP}} P_{MPP}(t).dt} \tag{33}$$

Table III presents the average dynamic MPPT tracking efficiency values of the proposed MPPT technique. This latter could achieve excellent performance under dynamic irradiation changes including rapid convergence speed, reduced power oscillations and alleviated power losses, which leads to enhanced PV power tracking efficiency.

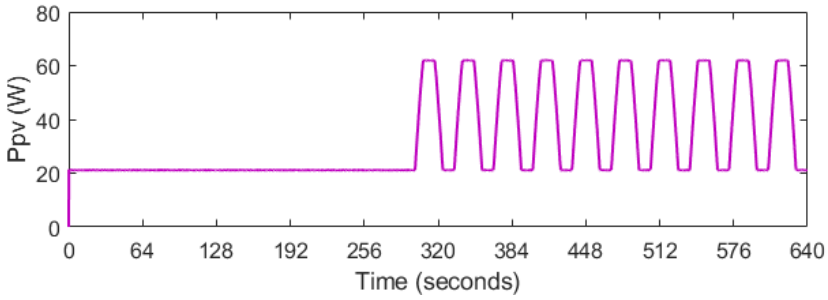

Fig. 10. Dynamic test sequences results according to EN50530 standard

Table III: Average dynamic MPPT tracking efficiency

Irradiance variation	$\eta_{dyn,MPPT}$ (%)
10% to 50%	99.42
30% to 100%	99.57
1% to 10%	98.96

III. 1.2.Comparison of the proposed and existing MPPT techniques

The performance of the proposed MPPT technique is evaluated with respect to different existing techniques, namely P&O [3], modified incremental conductance (MIC) [26], particle

swarm optimization (PSO) [6], and a hybrid scheme combines P&O with fractional-order proportional-integral (P&O-FOPI) [27]. These techniques are selected on purpose to compare the effectiveness of the proposed one: P&O represents the conventional type; MIC is the conventional type with an adaptive feature; PSO represents the metaheuristic algorithm; while P&O-FOPI is the hybrid MPPT control types. The simulation parameters including sampling time and switching frequency are selected the same for all techniques in order to have a fair comparison. The proposed MPPT method is first compared to the PSO in simulation under constant conditions (1000W/m² and 25°C) as shown in Fig.11 (a). The results reveal that the PSO method provides proper steady-state operation with negligible PV power disturbance. However, compared to the proposed method, the PSO algorithm faces considerable overshoots and has a very slow convergence speed (2.8s) to be used under rapid varying sun irradiance. The other MPPT techniques have been tested in simulation under varying solar irradiance and ambient temperature (25°C). The solar irradiance profile applied to the PV system is presented in Fig. 11 (b). It contains four irradiance intensities applied successively for 100ms each. The MPPT algorithm's behavior is tested under high and low irradiance levels, from 600W/m² to 1000W/m² and from 100W/m² to 400W/m² respectively; as well as under large variation when irradiance level falls from 1000W/m² to 100W/m². The power tracking profiles of the proposed technique, P&O, MIC, and P&O-FOPI are depicted in Fig.11 (c).To have better clarification about the algorithm's behavior at the steady-state and the transients, some parts of the curves are zoomed in Images 1, 2, 3 and 4 of Fig.11. From the comparison plot, it can be observed that the developed MPPT control strategy demonstrated performance superiority. It has the shortest MPP tracking period, the least transient fluctuations, zero oscillation around MPP and high tracking accuracy so low power losses. While the conventional P&O method suffers from steady-state power oscillation and the reached average value of power is less than the true MPP. The MIC shows better tracking performances and lower oscillation in steady-state than P&O. The hybrid technique P&O-FOPI provides faster convergence and better accuracy in locating the MPP compared to P&O and MIC and can mitigate the P&O steady-state oscillations. Nevertheless, it appears from this comparison that the developed MPPT techniques exhibit the most attractive features to be used under rapid varying irradiance compared to other methods.

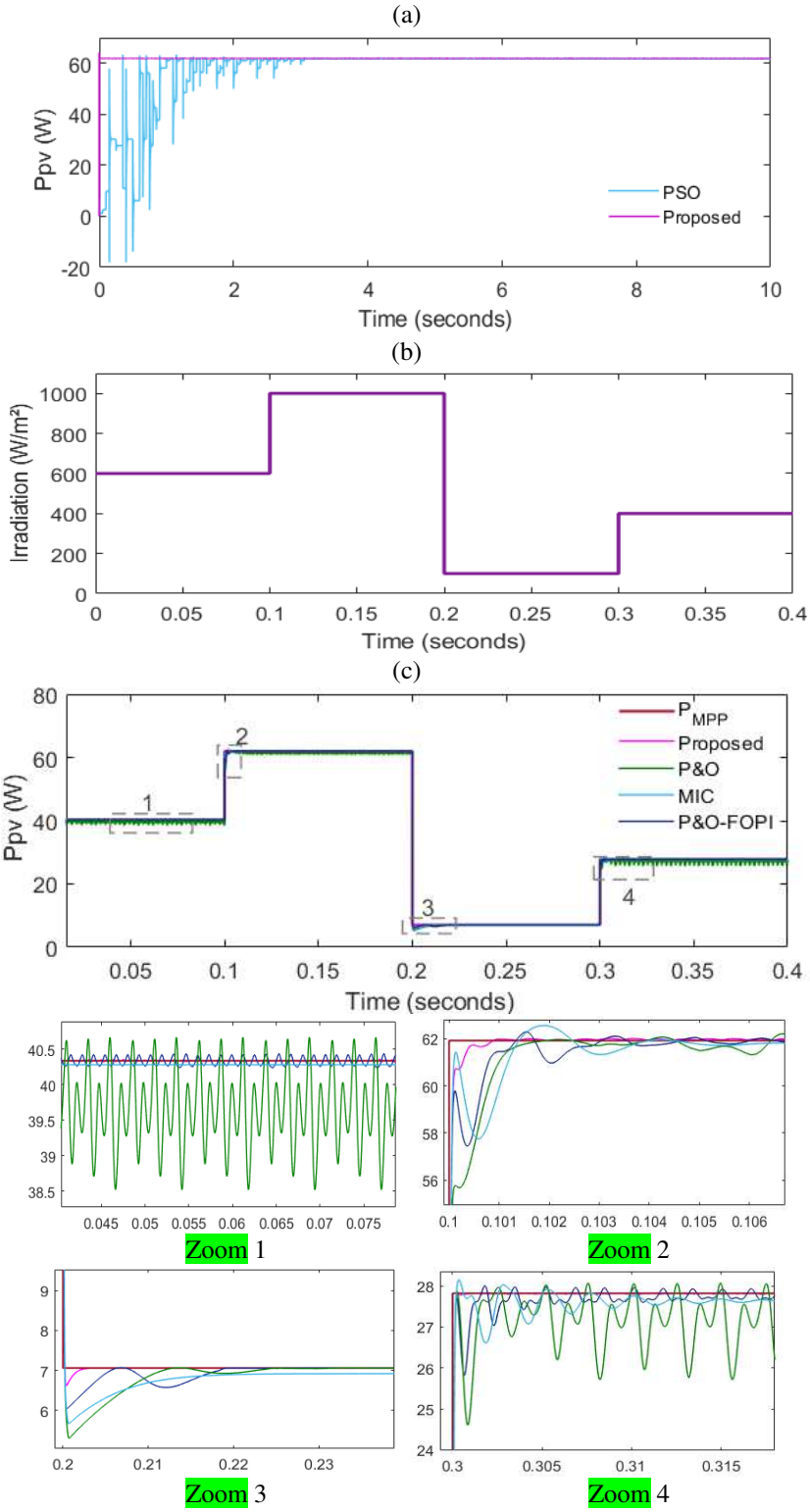

Fig. 11. Simulation comparison of MPPT algorithms (a) PSO versus the proposed (b) Sun irradiance profile (c) P&O, MIC and P&O-FOPI versus the proposed

III. 2. Experimental validation

III. 2.1. Experimental setup

Figure 12 depicts the experimental setup of the proposed MPPT technique. The experimental tests were conducted using the PV array already introduced and whose experimental I-V characteristic is presented above. The PV array was connected to the DC load (12V-120Ah batteries wired in series) via the boost converter with the parameters given in Table II. A dSPACE DS1104 platform is used to implement the proposed MPPT controller, which facilitates the real-time testing. The DS1104SL–DSP–PWM block is utilized to generate the desired PWM signal for the converter that is fed through the gate driver (IR2110) circuit. Voltages and currents are measured by employing resistor dividers and LA 25-NP sensors and then converted to digital signals using ADC interfaces of DSP that vary under a voltage range between -10V and +10V. PWM generation and instantaneous power schemes for the proposed MPPT controller in the dSPACE are illustrated in Fig.13. To get rid of high-frequency noise signals, the A/D channel output is passed through an analog filter. Before this block, a gain scale of 10 is added for dSPACE adaptation. The instantaneous power was calculated by multiplying the instant array current and voltage. The instantaneous array voltage and current, inductor current, and output voltage are provided to the input of the implemented MPPT algorithm to produce a duty cycle for the boost converter. It must be noted that the switching frequency chosen in this study was set depending on the interface DSP board limitation. It is generally recommended that the time-step used by the board (1µs in our case) be approximately 40 times smaller than the switching period of the converter, to ensure good precision and keep the results accurate [28].

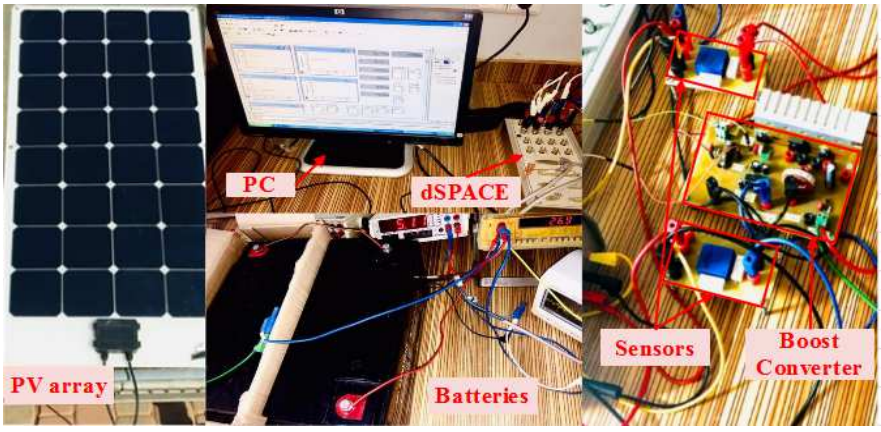

Fig.12. Laboratory experimental setup to implement the proposed MPPT technique

(a)

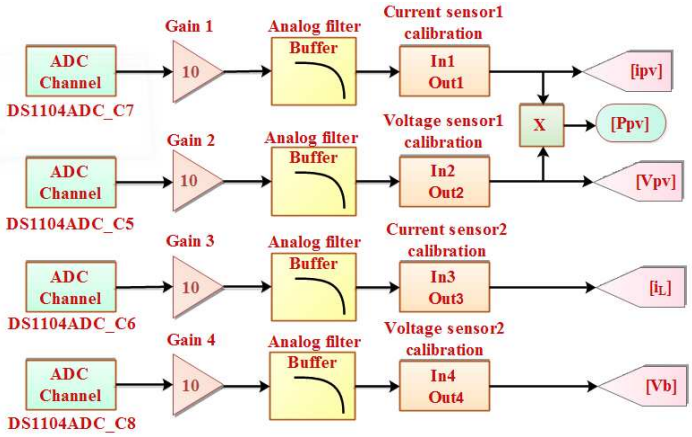

(b)

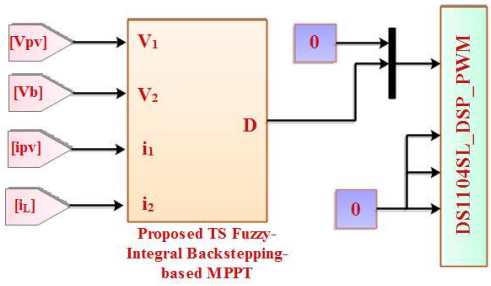

Fig. 13. dSPACE implementation scheme of MPPT algorithm (a) parameters measurement (b) PWM generation

III. 2.2. Experimental results and discussion

This section aims to experimentally demonstrate the good performance of the proposed MPPT technique helping in the PV system harvest maximization. The working of the PV battery charging system, as well as the MPPT control, has been firstly verified under steady-state operating conditions at 11:45 am on March 08, 2020, in Marrakech city: the sun irradiance was 950W/m² and the temperature was 24°C. Practically found responses of the voltage, current, and power provided by the PV panel are illustrated in Fig.14. Zoomed view of the PV power during the start-up transient is shown in Image 1 of Fig.14 to highlight how fast the convergence speed of the proposed controller (1.2s), which is one of the most rigorous features required under rapidly irradiation changing. The steady-state operation around the MPP is enlarged in Image 2 of Fig.14 showing stable behavior and high tracking efficiency. The proposed MPPT algorithm located the actual MPP accurately, which results in harvesting the maximum available power from the PV module ($P_{pv(max)}$≈59.46W) and achieving high tracking efficiency.

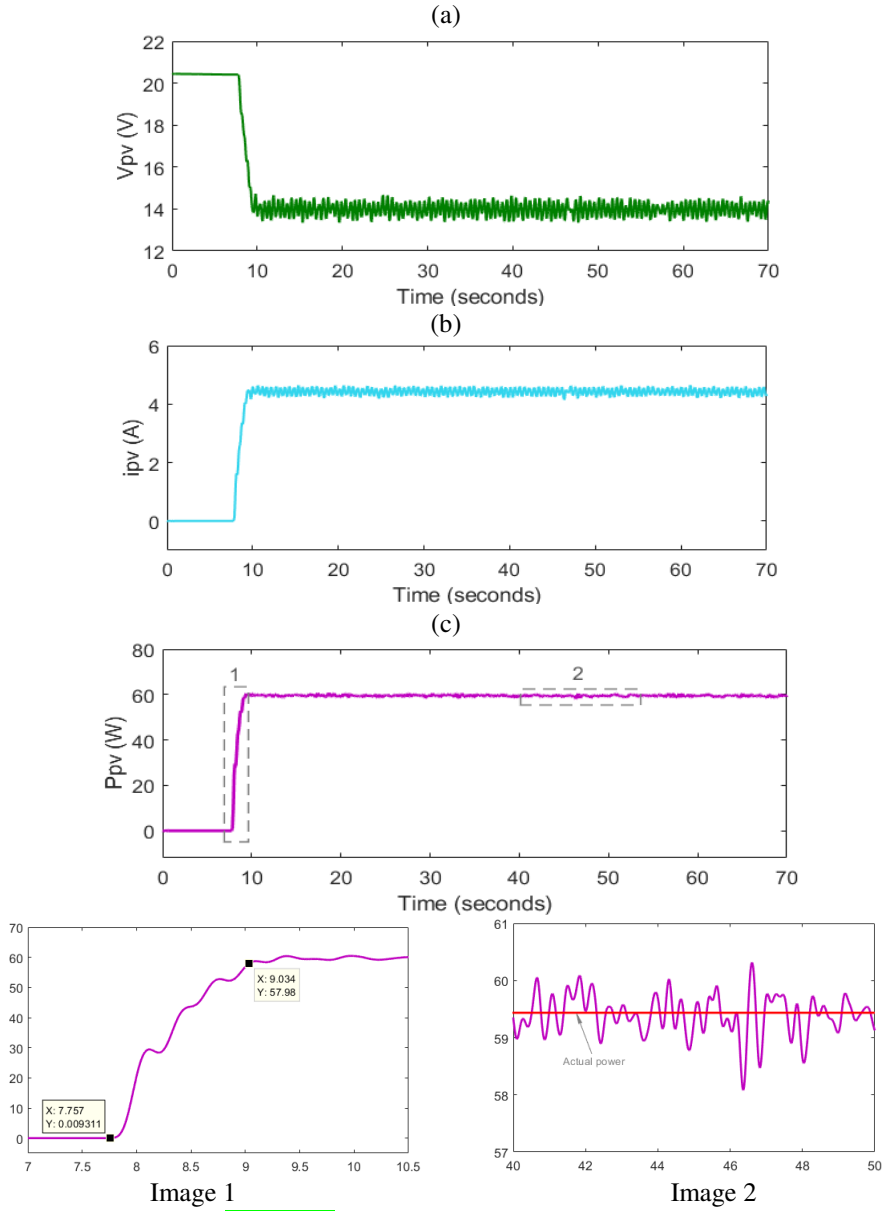

Fig. 14. Experimental results of the developed MPPT controller under steady-state conditions 950W/m², 24°C (at 11:45am on March 08, 2020 in Marrakesh city)(a)PV array voltage compared to reference voltage V_{pv}^{ref} (b) PV array current (d) produced power by the PV panel

The maximum power is successfully transmitted to the load throughout the boost converter. Figure 15 shows the measured waveform of the converter output terminals and reveals that the batteries kept charged as the maximum rated voltage constantly maintained.

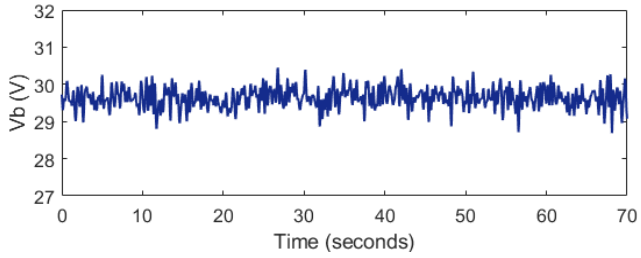

Fig. 15. Measured converter output voltage waveform

Fast sudden variations of irradiation level from sunshine to shade often happened naturally as a result of the shadow of buildings and tall tree species. The tracking performance and the robustness of the developed MPPT technique have been tested under a rapidly changing sun irradiation scenario. During the experiment, the PV array experienced a surface coverage to block the sunlight in different instants of time exemplifying the sharp irradiation changes encountered in reality. Experimental waveforms of PV voltage and PV power are captured confirming the effectiveness of the proposed TS Fuzzy-Integral Backstepping- based MPPT control as shown in Fig.16.The PV voltage tracks the reference voltage with high accuracy, which reveals the optimal working of the PV system control. It can be also observed from the PV power profile that despite the large abrupt perturbation of irradiance, the proposed MPPT controller has ensured fast convergence, high sensitivity to irradiance change, and negligible oscillations, which alleviate energy losses and guarantee higher dynamic tracking efficiency.

The behavior of the proposed MPPT controller has been also tested under the low sun irradiation profile presented in Fig.17 (a). Repeated step-up and step-down of irradiance level from 180W/m² to 500W/m² and vice-versa were applied during a period of 20s. Fig.17 (b) represents the excellent power tracking ability of the photovoltaic system using the proposed MPPT algorithm under dynamic changes of low irradiation levels. Stable operation with almost negligible power ripples at steady-state can be also observed. The results of this test demonstrated the precision in locating the right MPP position even for low irradiation levels, which is achieved owing to the TS fuzzy approach used in the proposed MPPT controller.

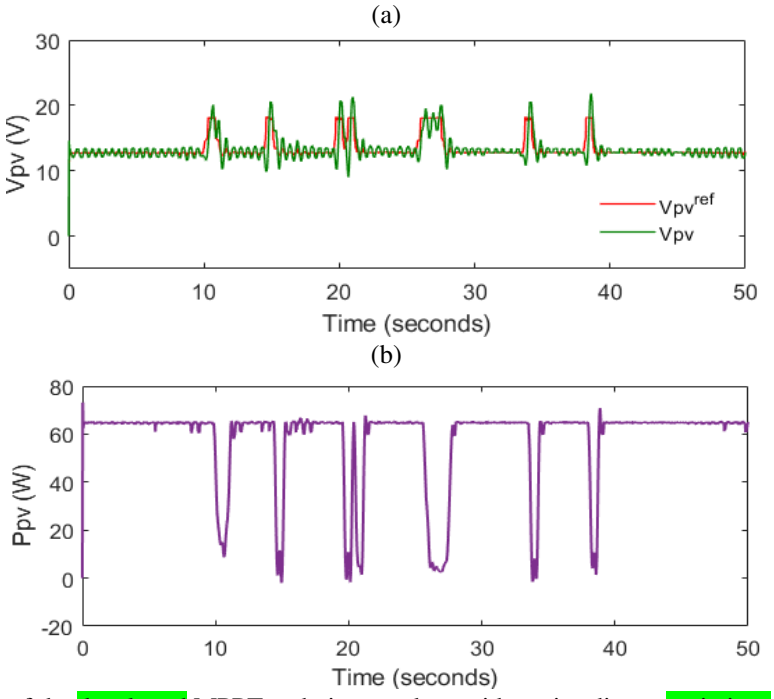

Fig. 16. Performance of the developed MPPT technique under rapid sun irradiance variations (a) PV array voltage compared to reference voltage V_{pv}^{ref} (b) generated power by the PV array

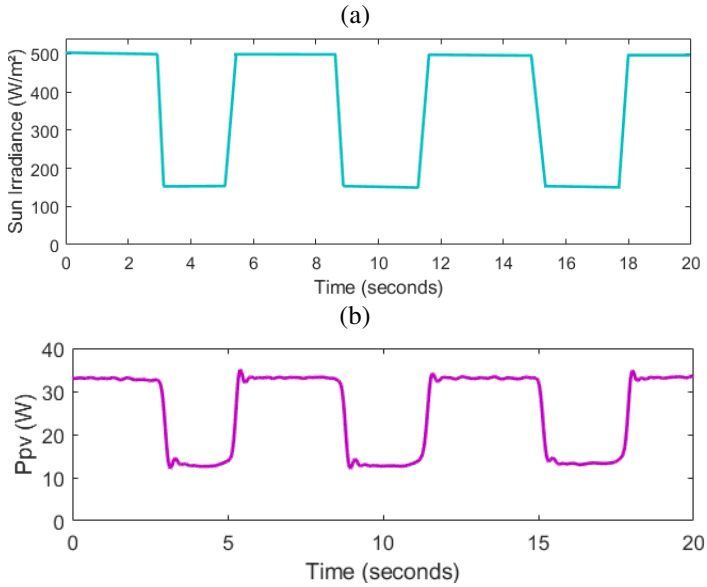

Fig. 17. Power tracking ability in low sun irradiance profile (a) Sun irradiance profile (b) generated power by the PV array

A comparative analysis is conducted to prove how MPPT control performances can be improved when using the integral backstepping method instead of the classical backstepping method [29]-[30]. The experimental test starts by adopting the classical backstepping in the MPPT algorithm, then, it is replaced by integral backstepping at the instant 28.95s. Figure 18 depicts the resulted PV voltage and PV power waveforms. PV voltage and reference voltage are plotted together as presented in Fig.18 (a), displaying a static error of 3.2V during the use

of the classical backstepping method, which results in power losses as shown in Fig.18 (b). Integral backstepping on the other hand completely removes the static error and tracks perfectly the peak power 60.02W. It is worth mentioning that the time *t* indicated in Fig.18 (a) does not present the settling time of the integral backstepping method but includes the upload time of its program. The obtained practical results reflect the importance of integral action in overcoming the classical backstepping drawbacks namely the static error.

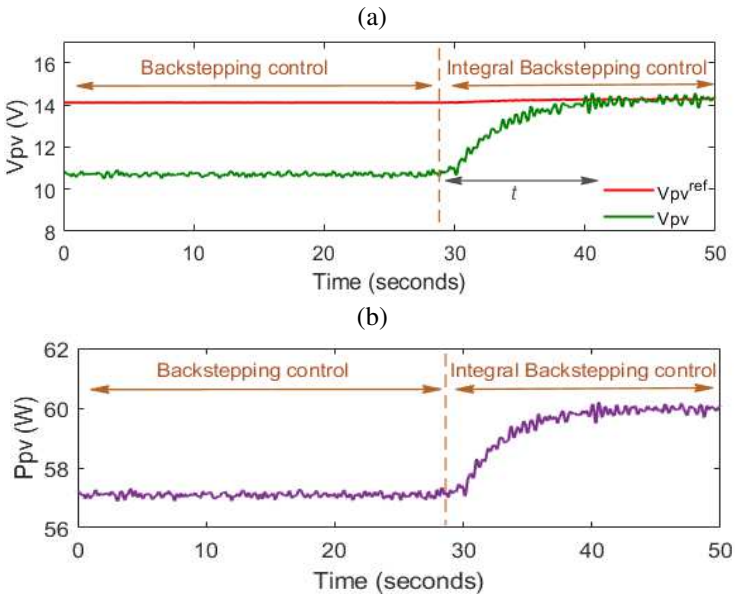

Fig. 18. Comparison of behavior of backstepping control and integral backstepping control (a) PV array voltage compared to reference voltage V_{pv}^{ref} (b) generated power by the PV module

The effectiveness of the proposed MPPT method has been validated through experimental comparison with the P&O algorithm under steady-state and dynamic conditions as presented in Fig.17. Due to the steady-state oscillation problem that can negatively affect the circuit, the P&O step size was carefully selected to get an optimal working of the method. Even though, practical results are shown in Fig.19 (a) interpret that the developed MPPT technique has a better response (higher tracking accuracy, faster dynamic, and less PV power steady-state oscillation) compared to the P&O technique. Owing to the considerable amount of time taken to attain the MPP, the P&O algorithm has shown very weak tracking performances under successive solar irradiance level change as depicted in Fig.19 (b). The presented results strongly confirm the reliable behavior of the proposed MPPT method under fluctuating sun irradiance addressed before (Fig.16 (b)).

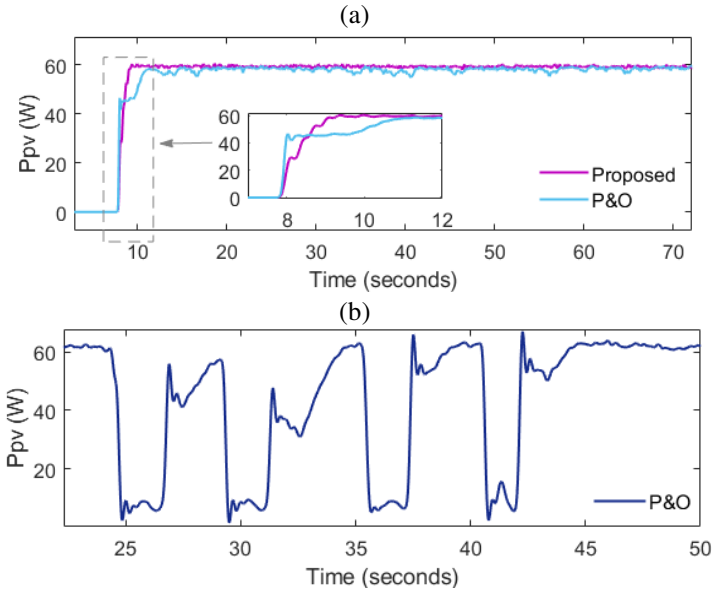

Fig. 19. P&O algorithm (a) under steady-state conditions (at 11:45am on March 08, 2020 in Marrakech city) (b) dynamic behavior under sudden variations of solar irradiance

IV. Conclusion

In this paper, an MPPT controller, combining the TS Fuzzy and integral backstepping methods, used for a boost-type solar charging battery system is proposed. The TS Fuzzy technique is essentially utilized to ensure the prediction of the MPP; while the integral backstepping method guarantees the efficient MPP tracking and the global asymptotic stability of the system that is demonstrated throughout Lyapunov stability criteria. The modeling and control analysis have been used to synthesize enhanced MPPT controller performances in terms of transient and steady-state responses. According to the obtained simulation and experimental results, the developed MPPT control strategy successfully deals with different dynamic irradiance changes and provides attractive features such as rapid tracking convergence velocity, accuracy in locating the MPP, reduced steady-state oscillations, and high tracking efficiency. The implemented research work is a significant contribution for improving the PV power generation under highly dynamic irradiance variation by using an efficient MPPT technique. As a future scope, it would be interesting to improve the overall photovoltaic system efficiency by improving the power converter topology. The DC/DC multilevel converter type would be a good candidate to achieve high step-up ability and reduced switching losses.

Acknowledgments

This research work was financially supported by the PHC Toubkal project (20/103-N°43692PB) and the CNRST Morocco.

References

[1] Lyden S, Haque M.E. Maximum Power Point Tracking techniques for photovoltaic systems: A comprehensive review and comparative analysis. Renewable and Sustainable Energy Reviews 2015; 1504–1518. https://doi.org/10.1016/j.rser.2015.07.172

[2] Thakran S, Singh J, Garg R, Mahajan P. Implementation of P&O Algorithm for MPPT in SPV System", IEEE International Conference on Power Energy. Environment and Intelligent Control (PEEIC) Greater Noida, India; 2018. https://doi.org/10.1109/PEEIC.2018.8665588

[3] Loukriza A, Haddadia M, Messaltib S. Simulation and experimental design of a new advanced variable step size Incremental Conductance MPPT algorithm for PV systems. ISA Transactions 2016; 62, 30-38. https://doi.org/10.1016/j.isatra.2015.08.006

[4] Megantoro P, Dwi Nugroho Y, Anggara F, Suhono, Yuniarti Rusadi E. Simulation and Characterization of Genetic Algorithm Implemented on MPPT for PV System under Partial Shading Condition. IEEE 3rd International Conference on Information Technology, Information System and Electrical Engineering (ICITISEE) Yogyakarta, Indonesia; 2018. https://doi.org/10.1109/ICITISEE.2018.8721031

[5] Zeddini M. A, Pusca R, Sakly A., Mimouni M. F. PSO-based MPPT control of wind-driven Self-Excited Induction Generator for pumping system. Renewable Energy 2016; 95: 162-177. https://doi.org/10.1016/j.renene.2016.04.008

[6] Sundareswaran K., Peddapati S., Palani S. Application of random search method for maximum power point tracking in partially shaded photovoltaic systems. IET Renewable Power Generation 2014; 8 (6): 670 - 678. https://doi.org/10.1049/iet-rpg.2013.0234

[7] Kumar Sahoo S, Balamurugan M, Anurag S, Kumar R, Priya V. Maximum power point tracking for PV panels using ant colony optimization. IEEE Innovations in Power and Advanced Computing Technologies (i-PACT); 2017. https://doi.org/10.1109/IPACT.2017.8245004

[8] Mao M, Zhang L, Duan P, Duan Q, Yang M. Grid-connected modular PV-Converter system with shuffled frog leaping algorithm based DMPPT controller. Energy 2018; 143 : 181-190. https://doi.org/10.1016/j.energy.2017.10.099

[9] Farajdadian S, Hassan Hosseini S. M. A new MATLAB/Simulink model of triple-junction solar cell and MPPT based on artificial neural networks for photovoltaic energy systems. Ain Shams Engineering Journal 2015; 6(3): 873-881. https://doi.org/10.1016/j.asej.2015.03.001

[10] Verma P., Garg R., Mahajan P. Asymmetrical interval type-2 fuzzy logic control based MPPT tuning for PV system under partial shading condition. ISA Transactions 2020; 100: 251-263. https://doi.org/10.1016/j.isatra.2020.01.009

[11] Ben Salah C., Ouali M. Comparison of fuzzy logic and neural network in maximum power point tracker for PV systems. Electric Power Systems Research 2011; 81(1): 43–50. https://doi.org/10.1016/j.epsr.2010.07.005

[12] Eltamaly A. M, Abdelaziz A. Y. Modern Maximum Power Point Tracking Techniques for Photovoltaic Energy Systems. Springer International Publishing. Cham: Switzerland; 2019. https://doi.org/10.1007/978-3-030-05578-3

[13] Farhat M, Barambones O, Sbita L. A new maximum power point method based on a sliding mode approach for solar energy harvesting. Applied Energy 2017; 185: 1185- 98. https://doi.org/10.1016/j.apenergy.2016.03.055

[14] Menaga D, Sankaranarayanan V. A novel nonlinear sliding mode controller for a single stage grid-connected photovoltaic system. ISA Transactions 2020. https://doi.org/10.1016/j.isatra.2020.07.021

[15] Pradhan R, Subudhi B. Double Integral Sliding Mode MPPT Control of a Photovoltaic System. IEEE Transactions on Control Systems Technology 2016; 24(1): 285–292. https://doi.org/10.1109/tcst.2015.2420674

[16] Chatrenour N, Razmi H, Doagou-Mojarrad H. Improved double integral sliding mode MPPT controller based parameter estimation for a stand-alone photovoltaic system. Energy Conversion and Management 2017; 139: 97–109. https://doi.org/10.1016/j.enconman.2017.02.055

[17] Kihal A, Krim F, Laib A, Talbi B, Afghoula H. An improved MPPT scheme employing adaptive integral derivative sliding mode control for photovoltaic systems under fast irradiation changes. ISA Transactions 2018; 87: 297-306. https://doi.org/10.1016/j.isatra.2018.11.020

[18] Salimi M. Practical implementation of the Lyapunov based nonlinear controller in DC-DC boost converter for MPPT of the PV systems. Solar Energy 2018; 173: 246–255. https://doi.org/10.1016/j.solener.2018.07.078

[19] Pathak, D., Sagar, G., & Gaur, P. (2020). An Application of Intelligent Non-linear Discrete-PID Controller for MPPT of PV System. Procedia Computer Science, 167, 1574–1583. https://doi.org/10.1016/j.procs.2020.03.368

[20] Abdel-Rahim O. A New High Gain DC-DC Converter with Model-Predictive-Control Based MPPT Technique for Photovoltaic Systems. CPSS Transactions on Power Electronics and Applications 2020; 5(2):191–200. https://doi.org/10.24295/cpsstpea.2020.00016

[21] Arsalan M, Iftikhar R, Ahmad I, Hasan A, Sabahat K, Javeria A. MPPT for photovoltaic system using nonlinear backstepping controller with integral action. Solar Energy 2018; 170: 192–200. https://doi.org/10.1016/j.solener.2018.04.061

[22] Elzein I. A, Petrenko Y. N. Assessing Under Varying Circumstances the Behavior of Photovoltaic Systems of Maximum Power Point Methods. International Journal of Smart Grid and Sustainable Energy Technologies 2019; 1(2): 45-51. https://doi.org/ 10.36040/ijsgset.v1i2.210

[23] Rhouma M. B. H, Gastli A, Ben Brahim L, Touati F, Benammar M. A simple method for extracting the parameters of the PV cell single-diode model. Renewable Energy 2017; 113: 885–894. https://doi.org/10.1016/j.renene.2017.06.064

[24] Zhou Z, Yu C, Teo K. L. Some New Results on Integral-Type Backstepping Method for a Control Problem Governed by a Linear Heat Equation. IEEE Transactions on Automatic Control 2017; 62(7): 3640–3645. https://doi.org/10.1109/tac.2017.2671778

[25] Alonso M, Chenlo F. Testing microinverters according to EN50530. 29th EU PVSEC Amsterdam, The Netherlands; 2014.

[26] Tey K. S, Mekhilef S. Modified incremental conductance MPPT algorithm to mitigate inaccurate responses under fast-changing solar irradiation level. Solar Energy 2014; 101: 333–342. https://doi.org/10.1016/j.solener.2014.01.003

[27] Yang B, Yu T, Shu H, Zhu D, An N, Sang Y, Jiang L. Energy reshaping based passive fractional-order PID control design and implementation of a grid-connected PV inverter for MPPT using grouped grey wolf optimizer. Solar Energy 2018, 170: 31–46. https://doi.org/10.1016/j.solener.2018.05.034

[28] Toh C. L, Idris N. R. N, Yatim A. H. M. Constant and High Switching Frequency Torque Controller for DTC Drives. IEEE Power Electronics Letters 2005; 3(2): 76–80. https://doi.org/10.1109/LPEL.2005.851316

[29] Hua Ch, Feng G, Guan X. Control of an Off-Grid PV System based on the Backstepping MPPT Controller. 13th International Conference Interdisciplinarity in Engineering INTER-ENG 2019, TarguMures, Romania; 46: 715-723. https://doi.org/ 10.1016/j.promfg.2020.03.101

[30] Martin A. D, Cano J. M, Medina-Garcia J, Gomez-Galan J. A, Vazquez J. R. Centralized MPPT Controller System of PV Modules by a Wireless Sensor Network. IEEE Access 2020; 8: 71694–71707. https://doi.org/10.1109/ACCESS.2020.2987621